



ORIGINAL ARTICLE

Ca²⁺ Signals in Astrocytes Facilitate Spread of Epileptiform Activity

Kjell Heuser¹, Cecilie G. Nome², Klas H. Pettersen³, Knut S. Åbjørnsbråten³, Vidar Jensen³, Wannan Tang³, Rolf Sprengel⁴, Erik Taubøll^{1,2}, Erlend A. Nagelhus^{1,3} and Rune Enger ^{1,3}

¹Department of Neurology, Oslo University Hospital, Rikshospitalet, N-0027 Oslo, Norway, ²Institute of Clinical Medicine, Faculty of Medicine, University of Oslo, N-0318 Oslo, Norway, ³Letten Centre and GliaLab, Division of Physiology, Department of Molecular Medicine, Institute of Basic Medical Sciences, University of Oslo, N-0317 Oslo, Norway and ⁴Max Planck Research Group “Molecular Neurobiology” at the Institute for Anatomy and Cell Biology, Heidelberg University, D-69120 Heidelberg, Germany

Address correspondence to Rune Enger and Erlend A. Nagelhus, Department of Molecular Medicine, Institute of Basic Medical Sciences, University of Oslo, PO Box 1103, Blindern, N-0317 Oslo, Norway. Email: rune.enger@medisin.uio.no and e.a.nagelhus@medisin.uio.no.  orcid.org/0000-0001-9418-7117

Kjell Heuser and Cecilie Nome contributed equally to this study.

Abstract

Epileptic seizures are associated with increased astrocytic Ca²⁺ signaling, but the fine spatiotemporal kinetics of the ictal astrocyte–neuron interplay remains elusive. By using 2-photon imaging of awake head-fixed mice with chronic hippocampal windows we demonstrate that astrocytic Ca²⁺ signals precede neuronal Ca²⁺ elevations during the initial bout of kainate-induced seizures. On average, astrocytic Ca²⁺ elevations preceded neuronal activity in CA1 by about 8 s. In subsequent bouts of epileptic seizures, astrocytes and neurons were activated simultaneously. The initial astrocytic Ca²⁺ elevation was abolished in mice lacking the type 2 inositol-1,4,5-trisphosphate-receptor (*Itpr2*^{-/-}). Furthermore, we found that *Itpr2*^{-/-} mice exhibited 60% less epileptiform activity compared with wild-type mice when assessed by telemetric EEG monitoring. In both genotypes we also demonstrate that spreading depression waves may play a part in seizure termination. Our findings imply a role for astrocytic Ca²⁺ signals in ictogenesis.

Key words: calcium signaling, epilepsy, glia, hippocampus, IP3R2, seizure, 2-photon

Introduction

Epileptic seizures are characterized by localized or spreading hypersynchronous neuronal activity. The mechanisms underlying this synchronization remain poorly understood. Synaptic and nonsynaptic factors, electrical field transmission as well as astrocytes have been proposed to contribute (Fellin and Haydon 2005; Zhang et al. 2014; Henneberger 2017).

Astrocytes are the main type of glial cells in the CNS, and are about as numerous as neurons (Sherwood et al. 2006; Azevedo et al. 2009). The delicate processes of one single astrocyte could form dynamic contacts with tens of thousands of neurons (Bushong et al. 2002). Furthermore, astrocytes express ion channels, neurotransmitter receptors and transporters and are able to release neuroactive substances. Thus, they are

permitted to indirectly modify neuronal excitability by controlling extracellular ion concentration or regulating uptake of neurotransmitters or more directly take part in neuronal signal transduction by active release of signalling substances (Perea et al. 2009; Halassa and Haydon 2010).

The discovery that astrocytes can respond to different physiological and nonphysiological stimuli by intracellular or wave-like intercellular Ca²⁺ elevations provided the awareness of a new dimension of signal transduction in the brain (Agulhon et al. 2008; Leybaert and Sanderson 2012; Bazargani and Attwell 2016). Such glial Ca²⁺ transients could possibly trigger release of active substances such as glutamate, D-serine, and ATP (Perea and Araque 2005; Panatier et al. 2011; Perea et al. 2009, 2014).

Along with growing knowledge of astroglial function in the healthy brain, the role of dysfunctional astrocytes in the pathogenesis of neurological disorders, including epilepsy, is now increasingly recognized (Eid et al. 2004; Aronica et al. 2012; Binder et al. 2012; Carmignoto and Haydon 2012; Coulter and Eid 2012; Steinhäuser et al. 2012). Several lines of evidence suggest a role for astrocytes both in *epileptogenesis*—that is, development of a recurrent seizure phenotype—through malfunctioning reactive astrocytes (Bedner et al. 2015; Steinhäuser et al. 2016; Klein et al. 2018) and *ictogenesis*—that is, the processes of transition from the interictal state to a seizure—by contributing to neuronal synchronization and spread of epileptic activity (Tian et al. 2005; Gómez-Gonzalo et al. 2010; Henneberger 2017). The interaction between astrocytes and neurons at the very transition from the nonseizing to the seizing state, has been sparsely investigated and provided conflicting results (Tian et al. 2005; Fellin et al. 2006; Gómez-Gonzalo et al. 2010; Baird-Daniel et al. 2017). However, these studies were performed on either brain slices (Fellin et al. 2006; Gómez-Gonzalo et al. 2010) with perturbed connectivity and lack of long-range connections, or in vivo using anesthesia (Baird-Daniel et al. 2017), which has been shown to suppress astrocytic Ca²⁺ signaling (Thrane et al. 2012).

The objective of the study was to resolve whether astrocytic Ca²⁺ signals are implicated in the spread of epileptic activity. We set out to assess the spatiotemporal relation between astrocytic and neuronal Ca²⁺ signals during kainate-induced epileptic seizures in awake mice by doing 2-photon microscopy through chronic window implants to the hippocampus CA1 region. To assess the potential involvement of astrocytic Ca²⁺ signals in seizures we used knockout mice (*Itp2*^{-/-}) lacking the inositol-1,4,5-trisphosphate (IP₃) receptor 2 (IP3R2), which mediates Ca²⁺ release from the endoplasmic reticulum. IP3R2 is the predominant IP₃ receptor in astrocytes, and *Itp2*^{-/-} mice exhibit strongly attenuated astroglial Ca²⁺ signals (Foskett et al. 2007; Srinivasan et al. 2015). We also investigated the seizure susceptibility of the *Itp2*^{-/-} mouse model by EEG telemetry.

Materials and Methods

Animals

Male C57Bl/6J wild-type (WT) (Janvier Labs) and *Itp2*^{-/-} (*Itp2*^{tm1.1Chen}, MGI:3640970) (Li et al. 2005) mice of 10–14 weeks of age were used for the experiments. Adequate measures were taken to minimize pain and discomfort. Mice were housed on a 12 h light:12 h dark cycle (lights on at 8 AM), 1–4 mice per cage. All experimental groups contained at least 6 mice. Experiments were carried out in accordance with the guidelines published in the European Communities Council Directive of 24 November

1986 (86/609/EEC). All procedures were approved by the Animal Use and Care Committee of the Institute of Basic Medical Sciences, the Faculty of Medicine at the University of Oslo and the Norwegian Food Safety Authority (project number: FOTS 7128 and 11255).

Virus Production and Transfection

Serotype 2/1 recombinant adeno-associated viruses (rAAV) from plasmid constructs pAAV-GFAP-GCaMP6f (Chen et al. 2013; Enger et al. 2017) and pAAV-SYN-jRGECO1a (Dana et al. 2016), were generated as described (Tang et al. 2009), purified by AVB Sepharose affinity chromatography (Smith et al. 2009) following titration with real-time PCR (rAAV titers about 1.0–6.0 × 10¹² viral genomes/mL, TaqMan Assay, Applied Biosystems, Inc.). Approximately 1 week before the chronic hippocampal windows were made, 200 nL of a mixture of the two viruses was injected at coordinates anteroposterior +2.5 mm, lateral +2 mm relative to bregma, at 2 different depths: –900 and –1300 μm relative to the brain surface. Mice used for acute slice experiments were injected bilaterally. The mice were left for 3 more weeks for the fluorescent sensors to be expressed before imaging experiments were performed.

Implantation of Chronic Hippocampus Windows

Anesthesia was induced in a chamber containing 3% isoflurane in room air enriched with 50% pure oxygen and subsequently maintained by nose cone flowing 1–1.5% isoflurane on the same gas mixture. Body temperature was kept at 37 °C by a temperature-controlled heating pad. Buprenorphine 0.15 mg/kg was injected intraperitoneally, and the mice were left for 10 min before surgery started. The field was sterilized, and local analgesia was accomplished by injection of bupivacaine (5 mg/mL). The skull was exposed and cleaned. Grooves were cut by scalpel in a checkerboard pattern into the periosteum to strengthen the adhesion of the cyanoacrylate glue that was subsequently applied concomitantly to the attachment of a custom-made titanium head bar. A 2.5 mm craniotomy with center coordinates anteroposterior –2 mm, lateral +2 mm relative to bregma was created as previously described (Dombeck et al. 2010; Kaifosh et al. 2013; Lovett-Barron et al. 2014; Zaremba et al. 2017). In short, a dental drill was used to carefully carve a circular groove in the skull with intermittent air puffs for the removal of debris until approximately 0.1 mm of the bone thickness was left. The bone fragment and the dura was then removed. Subsequently, the cortex was carefully removed with a custom made suction device. Extreme care was taken when approaching the alveus of the hippocampus. The last remnants of the overlying commissural fibers of the corpus callosum were removed with a microspatula. A circular cover glass of 2.5 mm diameter was glued onto a stainless steel cylinder with a similar outer diameter and a height of 1.5 mm. Subsequently, a 200 μm silver wire was glued onto the side of the cylinder, so that it protruded approximately 200 μm below the level of the glass window, to enable local field potential (LFP) measurements. The cylinder was oriented so that the electrode was positioned approximately 2.6 mm posterior to bregma, and 1.3 mm lateral to the midline. Glue was applied to isolate everything but the very tip of the electrode. The cylinder was then centered in the craniotomy, and lowered so that the glass coverslip very slightly depressed the alveus of the hippocampus. The cylinder was subsequently fastened by cyanoacrylate gel glue and dental cement to the skull. An additional

silver wire placed epidurally on the contralateral hemisphere served as reference (200 μm diameter, noninsulated). Care was taken to insulate the wires with glue and dental cement. Connectors for the wires were fastened onto the head bar.

Implantation of Telemetric EEG Transmitters

In total, 10 WT and 10 *Itp2^{-/-}* mice were implanted with radio transmitter EEG recording devices (TA10EA-F20; Data Sciences International). After pre-emptive buprenorphine (0.15 mg/kg) mice were anesthetized with isoflurane (same protocol as above). For the implantation of transmitters, a small skin incision was made in the right abdominal region, and a subcutaneous skin pouch was prepared by blunt dissection. A tunnel for the leads was created by careful blunt dissection towards the cranium until reaching the midsagittal incision. Two small craniotomies were made, positioned bilaterally 1.5 mm from the sagittal suture and 1.9 mm posterior to bregma, and 2 stainless steel screws were inserted (screw length 2 mm; thread diameter 0.8 mm). The telemetric implant was placed into the pouch, and the 2 monopolar leads were connected to the screws. The attached leads were covered with conductive glue and dental cement. The exposed cranium was also covered with dental cement and edges were secured by tissue adhesive. Mice were returned to clean cages and kept warm until they recovered from anesthesia and given buprenorphine (0.15 mg/kg, subcutaneously) and meloxicam (2 mg/kg, subcutaneously) postoperatively for 2 days.

Electrophysiology

Acquisition of data was synchronized by custom-written LabVIEW software (National Instruments). The mice were monitored by infrared-sensitive video surveillance. We used a Multiclamp 700B amplifier with headstage CV-7B (Molecular Devices), and the signals were digitized by National Instruments PCIe-6351, X Series Multifunction DAQ (National Instruments). For seizure detection in mice with implanted radio transmitters, the cages were placed on radio receiver plates (RPC-1; Data Sciences International). The signals were recorded in Dataquest A.R.T. 4.00 Gold/Platinum software (Data Sciences International) and exported to MATLAB for analysis. Seizures were elicited by intraperitoneal injection of 10 mg/kg kainate. EEG was recording for 1 h after kainate injected, following 10 min of baseline recording. Artifacts were manually removed from the EEG traces, and a baseline period was defined. The EEG traces were normalized such that the baseline amplitudes were stretched from -1 to 1 . Spikes were detected by a custom-made MATLAB script. A spike was defined as a local maximum if the local maximum was the largest local maximum in between 2 subsequent local minima and the valley-to-peak amplitude of the local maximum and a subsequent local minimum was at least 2 normalized units. Any time point of the recording was characterized as being epileptiform or nonepileptiform in a fully automated algorithm when the instantaneous spike rate was above 0.4 Hz on a spike train that was convolved with a normalized Gaussian window of 5 s duration. This threshold was chosen as it performed well across trials in separating baseline activity and obviously pathological EEG activity. For illustrational purposes, spikes were convolved with a normalized Gaussian window with a duration of 60 s for Figure 4b,c. The evaluator was blind to genotype. EEG spectrograms were generated by using the MATLAB implementation of short-time

Fourier transform, *spectrogram()*. EEG power was quantified by the MATLAB function *bandpower()* in the frequency ranges delta (0–4 Hz), theta (4–8 Hz), alpha (8–13 Hz), beta (13–30 Hz), and gamma (> 30 Hz).

In Vitro 2-Photon Microscopy

Acute hippocampal slices were prepared 3–6 weeks after virus transduction. The mice were killed with isoflurane (Baxter) and brains were removed. Transverse slices of 400 μm thickness from the dorsal and middle portion of each hippocampus, were cut with a vibroslicer (Leica VT1200) fitted with a sapphire blade (Ted Pella) in artificial cerebrospinal fluid (ACSF) at 23–25 °C, bubbled with 95% O₂ and 5% CO₂, containing (in mM): 124 NaCl, 2 KCl, 1.25 KH₂PO₄, 2 MgSO₄, 1 CaCl₂, 26 NaHCO₃, and 12 glucose (all from Sigma-Aldrich). For all following procedures, the CaCl₂ concentration in the ACSF was 2 mM. The slices were then placed in an interface chamber at 32 °C to recover for at least 1 h. One slice was then transferred to a submerged recording chamber that was perfused with ACSF at 4.5 mL/min, 32 \pm 1 °C. Tetrodotoxin (TTX; 1 μM ; Tocris Bioscience) was added to the ACSF to block voltage-gated sodium channels and thereby block seizure activity. The tissue expressed the same combination of genetically encoded fluorescent indicators as in the in vivo study. A recording electrode (filled with ACSF, 4–8 M Ω) was placed in the CA1 stratum pyramidale to confirm a successful blockage on neuronal action potentials. We used an Axon Multiclamp 700B amplifier, Digidata 1440 digitizer and pClamp10 software (Molecular Devices) for recording and digitalizing LFPs. Similarly, the SYN-jRGECO1a signal was used to ascertain the actions of TTX. GCaMP6f fluorescence was recorded by a 2-photon laser scanning microscope (model Ultima IV; Prairie Technologies) with an XLPLN 25 \times WMP 1.05 NA water-immersion objective (Olympus). A Chameleon Vision II (Coherent) laser provided an excitation wavelength of 999 nm. After 5 min of baseline recording, kainate was added to the bath solution for 3.5 min at 3 different concentrations (0.5, 2, or 10 μM). Images of 180 \times 180 pixels, representing a field of view of \sim 180 \times 180 μm^2 were acquired at a frame rate of approximately 6 Hz.

In Vivo 2-Photon Microscopy

Fluorescence was recorded by 2-photon laser scanning microscopy as previously described (Enger et al. 2017). An excitation wavelength of 999 nm was used. The first imaging session was performed at least 3 weeks after implantation of the chronic imaging window, in all 4 weeks after the virus injection. By that time the tissue robustly expressed fluorescent indicators in both neurons and astrocytes. There were no obvious changes to tissue morphology and astrocytes did not exhibit reactive morphological changes. Mice were then trained for 2–3 days with handling and getting used to head fixation on the spherical treadmill before data collection commenced. Seizures were elicited by injection of 30 mg/kg kainate intraperitoneally. During imaging experiments, mice that exhibited convulsive seizures according to a Racine seizure score of 5 or running seizures were sacrificed. GCaMP6f or jRGECO1a fluorescence was captured in images of 300 \times 300 pixels of approximately 170 \times 170 μm^2 areas in the transition zone between stratum pyramidale and stratum oriens of CA1 of the hippocampus (approximately 200 μm below the hippocampal surface) with frame rates of approximately 50 Hz.

Image Analysis

Imaging data were corrected for motion artifacts using the NoRMCorre movement correction software (Pnevmatikakis and Giovannucci 2017). Image segmentations and analyses were then performed with custom-written MATLAB programs. Regions of interests (ROIs) defining astrocytic compartments were manually drawn over somata, processes, and endfeet of cells with typical astrocytic morphology in the GCaMP6f signal. Similarly, neuronal somata were segmented and signals were extracted from both channels. The relative change in mean fluorescence ($\Delta F/F_0$) over time was calculated for each region of interest and subsequently analyzed by custom-written MATLAB scripts. The $\Delta F/F_0$ signal was filtered to remove noise with a moving average filter of 0.75 s duration. Subsequently, the built-in MATLAB function *findpeaks()* was applied to detect events (inspired by Barrett et al. 2018). A threshold of 0.5 and prominence height of 0.5 was used for the *findpeaks()* algorithm. Epileptic bouts were defined by synchronous elevations of the neuronal Ca²⁺ signals, where more than 80% of neuronal ROIs exhibited increased fluorescence simultaneously. Interictal astrocytic Ca²⁺ elevations were defined as astrocytic Ca²⁺ events (detected with same algorithm as above) that occurred outside the time points defined as epileptic. Additionally, an unbiased description of fluorescent events was performed by extracting signals from an evenly spaced grid of ROIs of 15 × 15 areas. This approach allowed us to demonstrate if regions with no clear cellular structures that were not segmented manually, exhibited altered Ca²⁺ kinetics. We used a threshold of 10% of max $\Delta F/F_0$ to define the time lag between onset of astrocytic and neuronal Ca²⁺ increase. For the assessment of astrocyte–neuron lag using manually drawn ROIs, the time point of fluorescent increase in a given astrocyte was compared with the mean of the time points of fluorescent increase in the 3 closest neurons. Imaging data from acute brain slices were analyzed with unbiased grid ROIs as described above. To make raster plots of Ca²⁺ events before, during and after kainate application in slices, Ca²⁺ events were detected as described above, and the resulting “spike trains” were convolved with a Gaussian window of 30 s and sigma of 10 s. Mean event rate plots were calculated per slice and plotted (Supplementary Fig. S1).

Statistical Analysis

Statistical analyses were performed using generalized linear mixed effects model statistics in MATLAB. This method was chosen because of the hierarchical study design with observations grouped by mouse identity and genotype, and that such models take into account the dependency between observations by including nested variance terms. We set genotype as the predictor variable and included a random intercept for mouse identity. The gamma distribution was used for non-negative, nonzero continuous variables (signal amplitudes, durations, and area under the curve (AUC)) as this gave the best approximation of the data. For astrocyte–neuron time lags, a normal distribution was presumed. Similarly, a Poisson distribution was used for spike frequency data. All data are given as estimated fixed effects by the mixed effects model with corresponding standard errors and P-values. Model fit was evaluated by Akaike information criterion and Bayesian information criterion and the MATLAB function *compare()* was used to compare different fits. Spike rate and seizure rate from telemetric EEG data was compared with a 2-sample students t-test as these data were nonhierarchical (one observation per animal) and

appeared to be normally distributed upon inspection. An alpha-level of 0.05 was used to determine significance. Group sizes were chosen based on typical group sizes in the literature that should be able to reveal biologically significant differences.

Results

Strong Ca²⁺ Fluorescence in Astrocytes and Neurons During Bouts of Seizures

The first bout of epileptiform activity emerged in the microscope’s field-of-view approximately 15 min after kainate injection. Bouts of seizures were defined as times where more than 80% of neuronal ROIs exhibited elevated Ca²⁺ signals. We were able to discriminate neuronal (SYN-jRGECO1a) and astrocytic (GFAP-GCaMP6f) fluorescent signals by a combination of color and morphology as described previously (Enger et al. 2017). Prominent fluorescent signals were detected in both astrocytes and neurons in relation to ictal onset (max $\Delta F/F_0$ was $1.5 \pm 0.1/0.1$ and $1.9 \pm 0.2/0.2$ in neuronal and astrocytic somata, respectively; Figs 1c and 3a,b; Tables 1 and 2). Bouts of seizures lasted approximately 80 s, whereas astrocytic and neuronal Ca²⁺ transients during seizures lasted roughly 50 s (Figs 1c and 3a,b; Tables 1 and 2). The frequency of epileptic seizures were $0.20 \pm 0.06/0.09$ bouts/min and $0.11 \pm 0.04/0.05$ bouts/min in WT and *Itpr2*^{-/-} mice, respectively ($P = 0.15$, see Fig. 3a). During such bouts of seizures, astrocytic Ca²⁺ event frequency and amplitude were increased and decreased, respectively, in astrocytic processes compared with somata (see Fig. 3b and Table 2). Even though epileptiform activity in the LFP signal was present within a variable period of time of neuronal fluorescence increases, the electrophysiological signals did not always concur with neuronal fluorescence. The reason for this is likely that the tip of the electrode was positioned some distance away (1–2 mm) from the field-of-view and because the low-resistance electrodes we used can detect signals over large distances when neuronal activity is highly synchronized (Lindén et al. 2011). The placement of a chronic LFP electrode within the field-of-view was not possible with the current hippocampal window preparation.

Astrocytic Ca²⁺ responses were strongly diminished in the *Itpr2*^{-/-} mice, underscoring that IP₃-mediated Ca²⁺ release from internal stores plays an important role in astrocytic Ca²⁺ dynamics during seizures. The fluorescent amplitudes during epileptic seizures in all glial ROI subtypes—somata, processes, and endfeet—were reduced by ~50% in the *Itpr2*^{-/-} mice (Fig. 3b, $P < 0.01$ for all comparisons). Similarly, the rate of Ca²⁺ transients was diminished ($P < 0.01$ for all comparisons). There was no significant reduction in duration and amplitude of neuronal Ca²⁺ responses in the *Itpr2*^{-/-} mice. However, the total AUC of the neuronal Ca²⁺ signal during seizures was reduced in the *Itpr2*^{-/-} mice, likely reflecting a less pronounced seizure burden ($101 \pm 10/20$ arbitrary units vs. $63 \pm 8/10$ arbitrary units, $P = 0.03$, Table 1).

Astrocytic Ca²⁺ Signals Precede Local Neuronal Ca²⁺ Activation at the Onset of Kainate-Induced Seizures

Surprisingly, the first cells to be activated locally in the field-of-view were always astrocytes. On average 8.4 ± 1.7 s after the astrocytic activation, fluorescence started to ramp up in neurons (Fig. 2a). Such preactivation of astrocytes was absent in the *Itpr2*^{-/-} mice ($P < 0.01$ and $P = 0.3$ compared with 0 s time lag, for WT and *Itpr2*^{-/-}, respectively; Fig. 2a). The astrocytic signals appeared in a synchronized fashion with no obvious

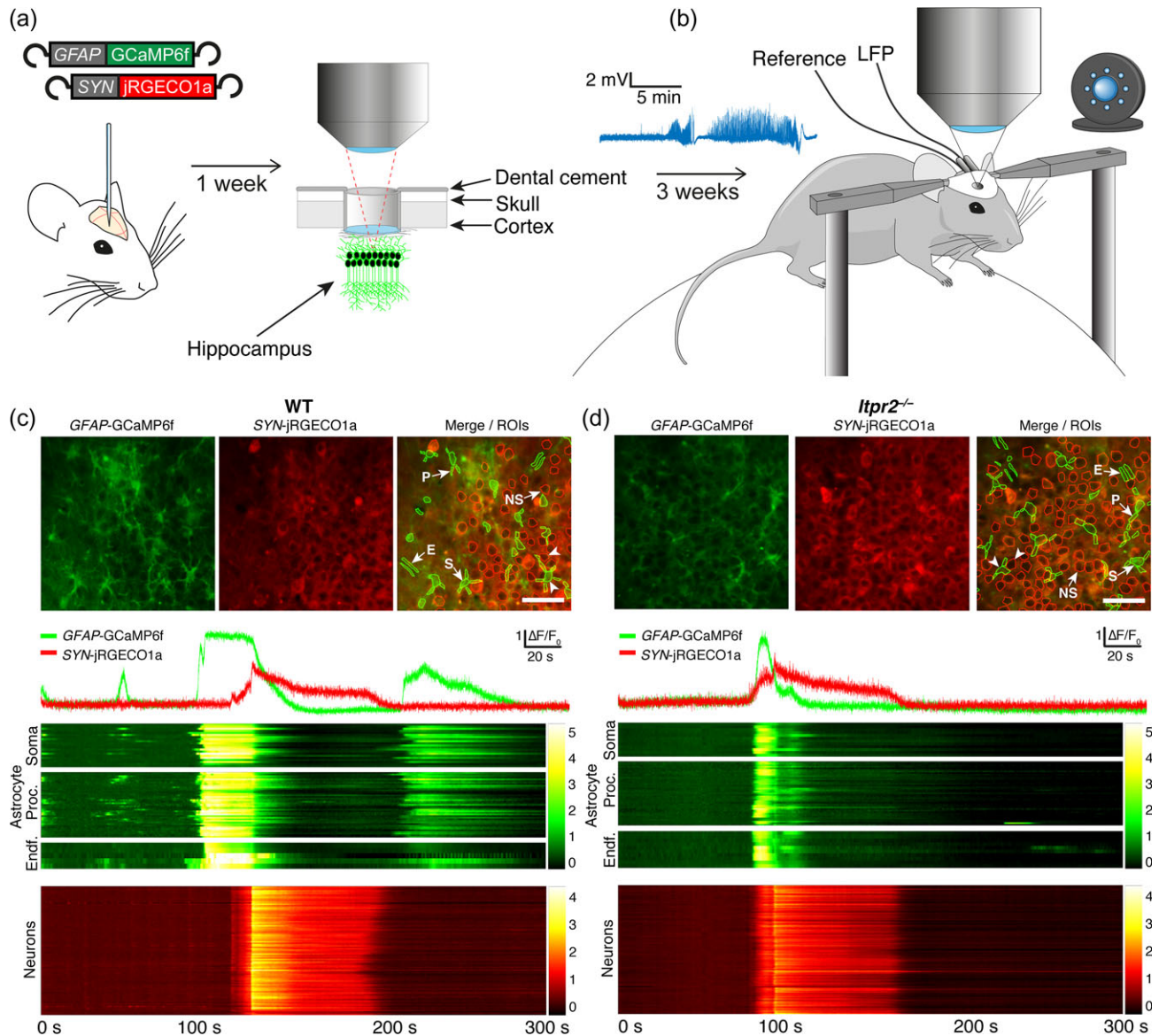


Figure 1. Simultaneous monitoring of neuronal and astrocytic Ca^{2+} levels during kainate-induced seizures. (a) Experimental setup and animal monitoring. First, a mixture of rAAV-GFAP-GCaMP6f and rAAV-SYN-jRGECO1a was injected in the right hippocampus. One week later, a 2.5 mm craniotomy was performed and the underlying cortical tissue was carefully removed, exposing the alveus of the hippocampus, followed by insertion of a cylinder with a glass mounted at the bottom and an LFP recording electrode. (b) The mice were left for at least 3 weeks before habituation to head-fixation commenced and the imaging experiment was performed. An infrared camera was used for animal monitoring during the imaging session. (c) Top row: Reference images from the hippocampal CA1 region, with ROIs plotted on the rightmost image: The arrows labeled S, P, and E indicate astrocytic somata, processes and endfeet, respectively; NS signifies neuronal somata. Second row: representative fluorescent traces from the ROIs marked with white arrowheads in the top row. Following rows: Temporal raster plots of fluorescent signals from all ROIs outlined in top row organized by ROI type. Each horizontal line represents fluorescence over time from a single ROI. (d) Similar to (c), but from an *Itpr2*^{-/-} mouse. Scale bars: 50 μm .

directionality (see Fig. 1c). Hence, it is unlikely that the observed Ca^{2+} elevation was a result of a Ca^{2+} wave spreading through the astrocyte syncytium. When manually drawing ROIs based on morphology, only a small portion of the total field-of-view is segmented. To assess whether smaller structures not readily distinguished by visual inspection displayed another fluorescent pattern than what we demonstrated above, we segmented the field-of-view into a 15×15 squares grid pattern. The resultant, evenly spaced grid of ROIs was covering the full field-of-view, and the ROIs were small enough to pick up activity in minor cellular subcompartments. In line with the analysis of manually segmented ROIs we found a clear preactivation of astrocytes

compared with neurons, and no consistent pattern of synchronous or asynchronous activity in the neuronal channel preceding the astrocytic activation. Similar to above, the astrocytic preactivation lasted 8.7 ± 1.7 s in WT mice and was absent in the *Itpr2*^{-/-} mice ($P < 0.01$ and $P = 0.43$ compared with 0 s time lag, for WT and *Itpr2*^{-/-}, respectively; Fig. 2b).

Notably, it was only during the first emergence of epileptiform activity the astrocytic Ca^{2+} signals preceded those of neurons. At later bouts of local epileptiform activity, astrocytes were activated concomitantly to neuronal signals or with varying time delays (astrocyte–neuron time lags were -4.1 ± 2.2 s and -3.1 ± 3.4 s in WT and *Itpr2*^{-/-} mice, respectively; $P = 0.76$

for comparisons between the 2 genotypes and $P = 0.06/0.23$, respectively, for WT and *Itpr2*^{-/-} mice compared with 0 s astrocyte–neuron time delay).

It seems unlikely that the initial preactivation could be due to direct activation of kainic acid receptors (KAR) on astrocytes, as there is no convincing evidence of expression of such receptors in bona fide astrocytes (Jabs et al. 1994; Vargas et al. 2013; Carta et al. 2014). To confirm the lack of functional expression of KARs on astrocytes, we performed a set of control experiments in acute brain slices expressing the same combination of fluorescent indicators as in the in vivo experiments, using TTX to block neuronal epileptiform activity. LFP recordings and concomitant expression of Ca²⁺ indicators in neurons confirmed a

successful blockage of neurons. Since kainate to a very little degree passes the blood–brain barrier (Gynther et al. 2015), only a small fraction of kainate reaches the brain interstitium following intraperitoneal administration. Typical doses that are sufficient to elicit epileptiform activity in slices are as low as, or even lower than, 500 nM (Ben-Ari and Cossart 2000). Hence, we performed our control experiments with 500 nM kainate concentration ($n = 10$ slices, 4 mice) concomitant to 2-photon microscopy of astrocytic responses. There was no increase in astrocyte Ca²⁺ event frequency or total AUC following kainate exposure (Supplementary Fig. S1). A subset of experiments were also carried out with 2 μ M kainate concentration ($n = 4$ slices, 2 mice) and 10 μ M kainate concentration ($n = 5$ slices, 2 mice), similarly demonstrating no increase in astrocyte Ca²⁺ signaling upon kainate application. Hence, a direct or in-direct activation of astrocytes through activity proximally in the mossy fiber-CA3-CA1 hippocampal trisynaptic circuit or other mechanisms are more likely to be the cause of the observed astrocytic preactivation.

Table 1 Neuronal Ca²⁺ dynamics.

| | WT | <i>Itpr2</i> ^{-/-} |
|--|--------------------|-----------------------------|
| Ca ²⁺ signal frequency (events/min/ROI) | 0.3 ± 0.04/0.04 | 0.2 ± 0.04/0.05 |
| <i>n</i> (Events, time, mice) | 9520, 5 h 46 m, 12 | 5420, 5 h 13 m, 6 |
| Duration (s) | 55.6 ± 7.0/10 | 45.4 ± 7.0/10 |
| <i>n</i> (Signals, ROIs, mice) | 7250, 3690, 12 | 4360, 2300, 6 |
| Amplitude ($\Delta F/F_0$) | 1.5 ± 0.1/0.1 | 1.2 ± 0.1/0.1 |
| <i>n</i> (Signals, ROIs, mice) | 7240, 3680, 12 | 4520, 2300, 6 |
| AUC (A.U.) | 100.9 ± 10/20 | 62.6 ± 8.0/10 |
| <i>n</i> (Signals, ROIs, mice) | 7300, 3680, 12 | 4490, 2400, 6 |

n = numbers in each group; ROI = region-of-interest; AUC = area under the curve; A.U. = arbitrary units.

Termination of the First Bout of Seizure

In all experiments, the first round of epileptiform activity was terminated by a prominent increase in the neuronal Ca²⁺ signal traveling as a wave through the field-of-view with a speed of 93 ± 9 μ m/s (Fig. 2c,e). The propagation speeds of these waves were significantly faster in the *Itpr2*^{-/-} mice (125 ± 13 μ m/s, $P = 0.049$). Both the speed and the amplitude of the signal in the neuronal channel suggested that the observed wave phenomenon was a

Table 2 Astroglial Ca²⁺ dynamics.

| | Seizure | | Interictal | |
|--|--------------------|-----------------------------|--------------------|-----------------------------|
| | WT | <i>Itpr2</i> ^{-/-} | WT | <i>Itpr2</i> ^{-/-} |
| Ca ²⁺ signal frequency (events/min/ROI) | | | | |
| Astrocyte somata | 0.3 ± 0.03/0.04 | 0.1 ± 0.02/0.02 | 0.2 ± 0.04/0.04 | 0.2 ± 0.03/0.04 |
| <i>n</i> (Events, time, mice) | 887, 5 h 42 m, 12 | 305, 5 h 4 m, 6 | 639, 5 h 42 m, 12 | 492, 5 h 4 m, 6 |
| Astrocyte processes | 0.4 ± 0.05/0.05 | 0.2 ± 0.03/0.03 | 0.3 ± 0.04/0.05 | 0.2 ± 0.04/0.05 |
| <i>n</i> (Events, time, mice) | 2440, 5 h 42 m, 12 | 722, 5 h 4 m, 6 | 1420, 5 h 42 m, 12 | 770, 5 h 4 m, 6 |
| Astrocyte endfeet | 0.3 ± 0.04/0.04 | 0.1 ± 0.03/0.03 | 0.2 ± 0.04/0.04 | 0.1 ± 0.03/0.04 |
| <i>n</i> (Events, time, mice) | 453, 5 h 42 m, 11 | 65, 5 h 4 m, 4 | 309, 5 h 42 m, 11 | 47, 5 h 4 m, 4 |
| Amplitude ($\Delta F/F_0$) | | | | |
| Astrocyte somata | 1.9 ± 0.2/0.2 | 1.1 ± 0.09/0.1 | 1.2 ± 0.06/0.07 | 0.8 ± 0.05/0.06 |
| <i>n</i> (Signals, ROIs, mice) | 460, 460, 12 | 269, 270, 6 | 646, 646, 12 | 141, 140, 5 |
| Astrocyte processes | 1.8 ± 0.2/0.2 | 1.0 ± 0.08/0.09 | 1.1 ± 0.06/0.07 | 0.8 ± 0.05/0.05 |
| <i>n</i> (Signals, ROIs, mice) | 1180, 1180, 12 | 642, 640, 6 | 1640, 1640, 12 | 400, 400, 5 |
| Astrocyte endfeet | 1.8 ± 0.2/0.2 | 0.9 ± 0.08/0.09 | 1.1 ± 0.06/0.07 | 0.8 ± 0.1/0.1 |
| <i>n</i> (Signals, ROIs, mice) | 233, 233, 11 | 57, 57, 4 | 304, 304, 11 | 15, 15, 3 |
| Duration (s) | | | | |
| Astrocyte somata | 55.3 ± 6.0/7.0 | 41.1 ± 6.0/8.0 | 6.0 ± 0.9/1.0 | 3.8 ± 0.6/0.9 |
| <i>n</i> (Signals, ROIs, mice) | 454, 454, 12 | 286, 290, 6 | 339, 339, 12 | 123, 120, 5 |
| Astrocyte processes | 56.5 ± 6.0/8.0 | 48.4 ± 8.0/10 | 5.6 ± 0.8/1.0 | 4.4 ± 0.7/1.0 |
| <i>n</i> (Signals, ROIs, mice) | 1180, 1180, 12 | 667, 670, 6 | 1030, 1030, 12 | 349, 350, 5 |
| Astrocyte endfeet | 57.8 ± 6.0/8.0 | 57.7 ± 20/40 | 7.1 ± 1.0/2.0 | 2.4 ± 0.6/1.0 |
| <i>n</i> (Signals, ROIs, mice) | 238, 238, 11 | 62, 62, 4 | 205, 205, 11 | 13, 13, 3 |
| AUC (A.U.) | | | | |
| Astrocyte somata | 72.0 ± 10/20 | 35.3 ± 5.0/6.0 | 16.6 ± 3.0/6.0 | 7.7 ± 1.0/2.0 |
| <i>n</i> (Signals, ROIs, mice) | 758, 758, 12 | 344, 340, 6 | 911, 911, 12 | 290, 290, 6 |
| Astrocyte processes | 72.4 ± 10/20 | 34.8 ± 4.0/6.0 | 15.7 ± 3.0/5.0 | 5.2 ± 0.6/0.8 |
| <i>n</i> (Signals, ROIs, mice) | 1880, 1880, 12 | 744, 740, 6 | 2360, 2360, 12 | 628, 630, 6 |
| Astrocyte endfeet | 72.9 ± 10/20 | 31.9 ± 4.0/5.0 | 16.6 ± 3.0/6.0 | 9.4 ± 2.0/4.0 |
| <i>n</i> (Signals, ROIs, mice) | 351, 351, 11 | 66, 66, 4 | 422, 422, 11 | 47, 47, 4 |

n = numbers in each group; ROI = region-of-interest; AUC = area under the curve; A.U. = arbitrary units.

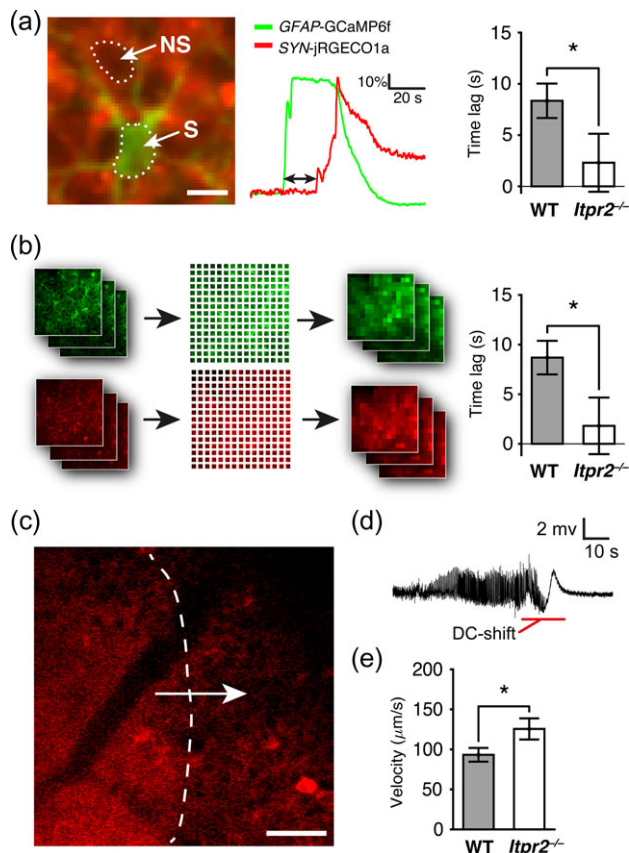


Figure 2. Astrocyte–neuron time lag and SD. (a) The GFAP-GCaMP6f fluorescence signifying astrocytic Ca^{2+} levels rose several seconds before fluorescence increased in the neurons. When using manually drawn ROIs, signals in astrocytic somata in WT mice preceded nearby neuronal somata by 8.4 ± 1.7 s. In *Itpr2*^{-/-} mice, the astrocyte–neuron lag was 2.3 ± 2.8 s. Signal start in the 2 channels was defined as the time point where fluorescence reached 10% of max $\Delta F/F_0$. NS = neuronal soma; S = astrocytic soma. Scale bar: $10 \mu\text{m}$. (b) Since manually drawn ROIs only segment parts of the total field-of-view, we opted for an automatic approach that segmented the field-of-view into a 15×15 grid pattern. The resultant evenly spaced ROIs were tentatively small enough to register low amplitude signals in small subcellular compartments. When analyzing these signals, the astrocytic GFAP-GCaMP6f signal preceded the neuronal SYN-jRGECO1a signal by 8.7 ± 1.7 s in WT. In *Itpr2*^{-/-} mice the astrocyte–neuron lag was 1.8 ± 2.9 s. (c) In all experiments, the first bout of epileptic activity was terminated by a fluorescent wave traveling through the field-of-view, whose speed and fluorescent waveform was similar to SD events. (d) Within 1–2 min of the fluorescent wave passing through the field of view, a characteristic DC shift was detected on the local field potential electrode. (e) The propagation speeds for the fluorescent waves were $93 \pm 9 \mu\text{m/s}$ and $125 \pm 13 \mu\text{m/s}$ for WT and *Itpr2*^{-/-} mice, respectively, $P = 0.049$. Scale bar: $50 \mu\text{m}$.

spreading depression (SD) event, and the faster propagation speed in the *Itpr2*^{-/-} is consistent with previously published data (Enger et al. 2017). There was a further increase in astrocytic Ca^{2+} fluorescence accompanying the SD events, typically following the neuronal fluorescent changes, but with a time delay of about 1 s, similar to what has previously been demonstrated in a pure SD model (Enger et al. 2017).

Although the LFP recording electrodes were not in immediate vicinity of the imaging field-of-view and the LFP signal was high-pass filtered (0.1 Hz), DC-shifts associated with spreading depolarizations were registered in a subset of experiments within a couple of minutes of the fluorescent waves. The wave phenomenon was followed by a period of quiescence in both recording channels. Within a few minutes, epileptiform activity re-emerged.

Interictal Ca^{2+} Activity in Astrocytes

Astrocytes also exhibited interictal “spontaneous” Ca^{2+} signals at times where no neuronal Ca^{2+} signals were detectable. These appeared at a rate of 0.3, 0.4 and 0.3 spikes per ROI per minute in somata, processes and endfeet, respectively (Fig. 3c and Table 2). They were of lower amplitude ($P < 0.001$ for all comparisons, Table 2) and shorter duration ($P < 0.001$ for all comparisons; Table 2) than during epileptiform activity. Astrocytic processes exhibited higher Ca^{2+} spike rates than somata ($P = 0.02$). Furthermore, there was a tendency towards a lower Ca^{2+} signal amplitude in processes compared with somata ($P = 0.05$). Both the signal amplitude and AUC of the astrocytic Ca^{2+} signals were reduced in the *Itpr2*^{-/-} mice ($P < 0.05$ for all comparisons, except AUC for the endfoot subcompartment where $P = 0.2$).

Seizure Characterization by Telemetric EEG Monitoring

In the Ca^{2+} imaging trials we observed a reduction in neuronal Ca^{2+} signal AUC in the *Itpr2*^{-/-} mice (see above). However, when doing 2-photon imaging in the hippocampus, we were not able to have a continuous monitoring of the mice for extended periods of time after kainate administration. Furthermore, the kainate dose used during 2-photon microscopy (30 mg/kg) may have been too high to clearly reveal differences between the 2 genotypes. Consequently, to assess whether seizure propensity differed between the 2 genotypes, we lowered the kainate dose and took advantage of chronically implanted EEG telemetry (Fig. 4a).

Both WT and *Itpr2*^{-/-} mice robustly developed seizures also with a low to moderate dose of kainate (10 mg/kg intraperitoneal). The seizure load was, however, markedly different in the 2 genotypes. Consistently, the *Itpr2*^{-/-} mice developed less epileptiform activity. In the 60 min recorded after kainate injection, WT mice had electrographic seizures on average $51 \pm 6\%$ of the time, compared with $19 \pm 5\%$ of the time in the *Itpr2*^{-/-} mice ($P < 0.01$; Fig. 4b–d). The spike rates were also markedly different in the 2 genotypes (75 ± 18 spikes/min vs. 30 ± 11 spikes/min, for WT and *Itpr2*^{-/-}, respectively, $P = 0.04$; Fig. 4d). Spectral analyses of the EEG signals revealed lower power in the beta and gamma frequency bands in the *Itpr2*^{-/-} mice (see Supplementary Fig. S2). For EEG spectrograms, see Supplementary Figure S1.

Discussion

Here, we used 2-photon microscopy and genetically encoded Ca^{2+} indicators to reveal Ca^{2+} signals in hippocampal astrocytes and neurons of awake mice during kainate-induced seizures. Strikingly, prominent astrocytic Ca^{2+} transients preceded local hypersynchronous neuronal activity during the initial bout of seizure activity. This phenomenon was abolished in *Itpr2*^{-/-} mice, indicating that the early astrocytic Ca^{2+} transients rely on IP3R2 mediated Ca^{2+} release from the endoplasmic reticulum. Furthermore, we report that *Itpr2*^{-/-} mice display less epileptic activity than WT mice, suggesting a proconvulsant role of astrocytic Ca^{2+} elevations. We also demonstrated that SD and epileptic activity coexist in both genotypes, and observed that SD reliably terminates local neuronal seizure activity.

The first cells to be activated locally in the field-of-view following intraperitoneal administration of kainate were always astrocytes. Their fluorescence increased several seconds before detectable synchronous activation of local neurons. This begs the question—what triggers the initial astrocytic activation?

Both the lack of convincing evidence of expression of KARs in bona fide astrocytes and our own slice experiments makes it highly unlikely that the observed preactivation is due to a

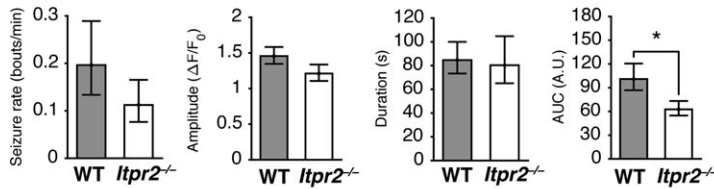
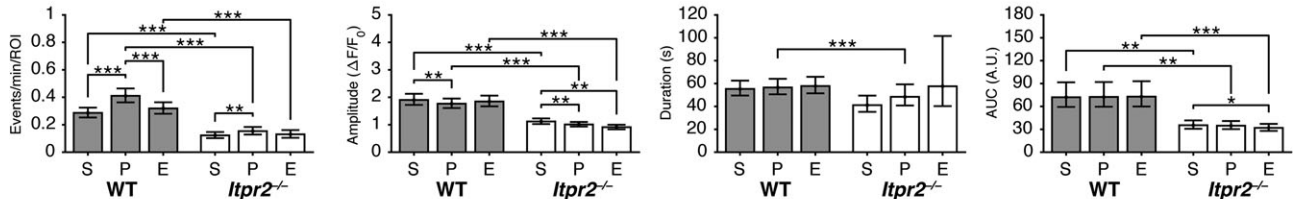
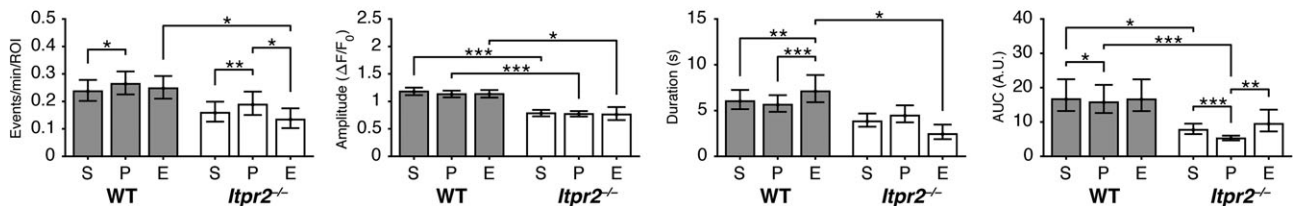
(a) Seizure characteristics based on neuronal Ca²⁺-signals(b) Astrocytic Ca²⁺-signals during seizure activity(c) Interictal astrocytic Ca²⁺-signals

Figure 3. Seizure characteristics and Ca²⁺ dynamics in astrocytes. (a) The rate, duration and amplitude of seizure bouts based on neuronal Ca²⁺ signalling were similar in the 2 genotypes, whereas the total area under the curve (AUC) of the neuronal Ca²⁺ signals was reduced in the *Itpr2*^{-/-} mice, compared with WT ($P = 0.02$). (b) *Leftmost panel:* The rate of astrocytic Ca²⁺ transients during bouts of seizures. *Middle left panel:* The amplitudes of astrocytic Ca²⁺ events during bouts of seizures. *Middle right panel:* The duration of astrocytic Ca²⁺ events during bouts of seizures. *Rightmost panel:* The AUC of astrocytic Ca²⁺ events during bouts of seizures. (c) Same as (b) but for interictal astrocytic Ca²⁺ events. See Tables 1 and 2 for group numbers. In (b) and (c), S, P, and E indicate astrocytic somata, processes, and endfeet, respectively.

direct effect of kainate on the astrocytes (Jabs et al. 1994; Vargas et al. 2013; Carta et al. 2014). However, the hippocampus displays a high density of KARs, and both light- and electron microscopy studies have demonstrated that KAR labeling primarily corresponds to presynaptic and postsynaptic mossy fiber synapses in particular in the CA3 region (Darstein et al. 2003; Ruiz 2005). Consequently, CA3 is thought to be the part of the hippocampus that is the most susceptible to low concentrations of kainate (Monaghan and Cotman 1982; Carta et al. 2014). As our field-of-view was limited to a circumscribed part of the CA1 region, it is highly improbable that we were able to directly detect the starting point of KAR mediated activation of the local hippocampal circuitry. Hence, it is likely that the observed initial astrocyte activation was directly or indirectly elicited by neuronal activity proximally in the mossy fiber-CA3-CA1 hippocampal trisynaptic circuit, although we cannot rule out direct ionotropic and metabotropic effects of kainate on the CA1 pyramidal neurons in the field-of-view (Melyan et al. 2002; Ruiz 2005; Carta et al. 2014). In line with this, it has been shown in numerous studies that astrocytic Ca²⁺ signals can be elicited by glutamatergic signaling (Porter and McCarthy 1996; Perea and Araque 2005; Schummers et al. 2008; Nimmerjahn et al. 2009).

Studies have demonstrated high activity in inhibitory neurons preceding local recruitment of excitatory neurons in seizures (Avoli and de Curtis 2011; Truccolo et al. 2011; Grasse et al. 2013; Toyoda et al. 2015; Khoshkhoo et al. 2017; Librizzi et al. 2017). Hence, the astrocytic preactivation could be mediated by activity in inhibitory neurons. Indeed, astrocytes have been shown to express both ionotropic and metabotropic GABA

receptors (Nedergaard and Verkhratsky 2012; Parpura and Verkhratsky 2013). However, we should have been able to detect activity in interneurons with our experimental setup, as the human SYNAPSIN-1 promoter is known to be expressed in both excitatory and inhibitory neurons (Nathanson et al. 2009). Even though our imaging plane was largely dominated by the excitatory neurons of stratum pyramidale, imaging planes were always placed obliquely to be able to pick up activity in stratum oriens—where we would expect to find more interneuron somata. Still, we found no evidence of neuronal activity concomitant to the astrocytic preactivation in any neuronal compartments in the field-of-view.

Long-range cholinergic (Takata et al. 2011; Chen et al. 2012) or noradrenergic (Bekar et al. 2008; Ding et al. 2013; Paukert et al. 2014) neuromodulatory projections have been shown to mediate coordinated Ca²⁺ signaling in astrocytes in the cortex. Most likely, hippocampal astrocytes could be activated in a similar fashion. Thus, also long-range neuromodulatory projections could mediate the astrocytic preactivation (Porter and McCarthy 1996; Perea and Araque 2005).

Given our findings, the concept of a role of astrocytes in the recruitment of neurons to seizure activity is tempting. Several known intrinsic astrocyte–neuron interactions can provide the underlying mechanisms, because of their ability to create excitatory feedback loops (Gómez-Gonzalo et al. 2010; Henneberger 2017). Astrocyte-mediated glutamate release and subsequent NMDA receptor stimulation has attracted most attention (Parpura et al. 1994; Tian et al. 2005; Crunelli and Carmignoto 2013), but other neuroactive molecules may also provoke

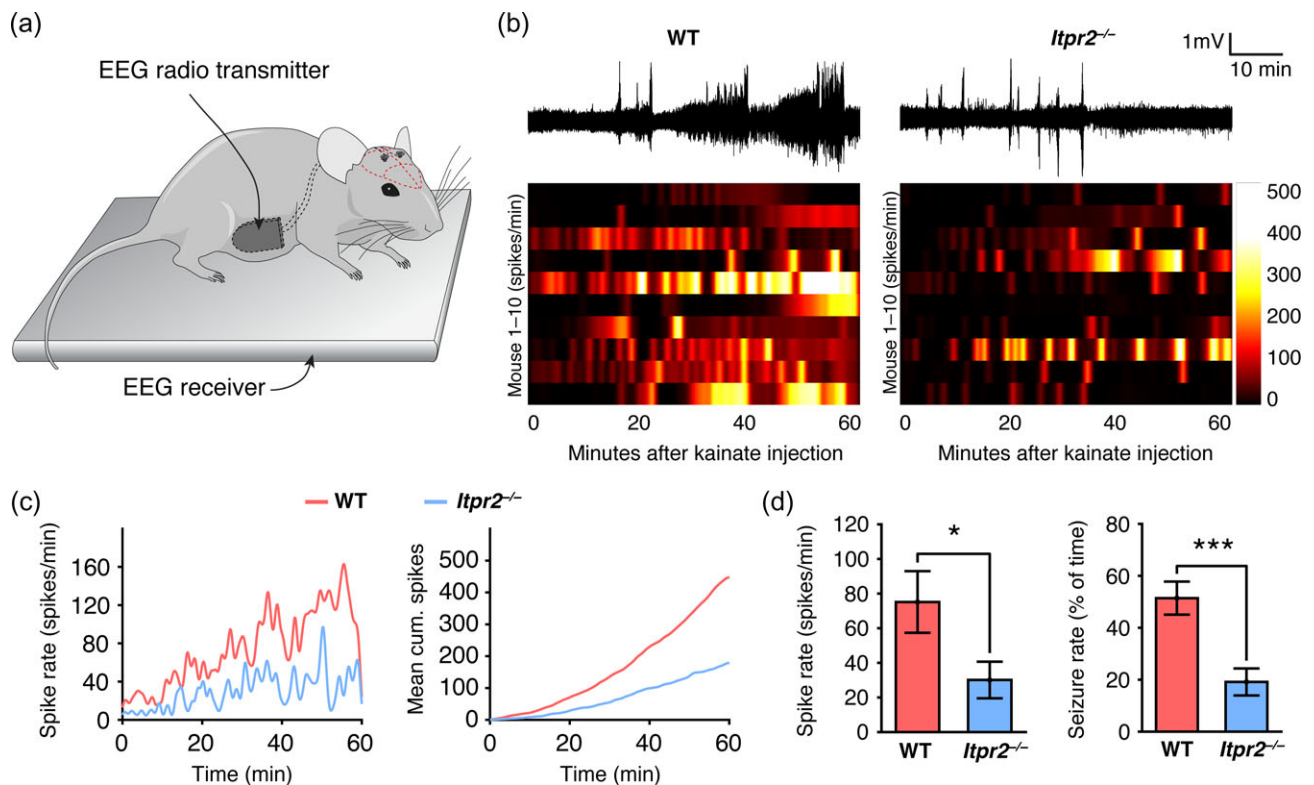


Figure 4. Seizure characterization by EEG telemetry. (a) EEG radio transmitters were implanted as illustrated. One week following, kainate (10 mg/kg) was administered intraperitoneally, and seizures were recorded by a radio receiver. (b) *Traces*: Representative EEG traces from the 2 genotypes. *Raster plots*: spike rates in all mice in both genotypes 60 min after kainate injection (c) *Left panel*: Mean spike rate over time for all mice in the 2 groups. *Right panel*: Cumulative spike count in the 2 genotypes. (d) *Left panel*: Mean spike rate in the 2 groups, $P = 0.04$. *Right panel*: Mean percentage of time the EEG is classified as epileptiform (see Materials and Methods), $P < 0.01$.

synchronization of local neuronal activity (reviewed in (Perea et al. 2009)). Our observation that *Itpr2*^{-/-} seemingly have differential effects on SD (higher propagation speed) and seizure activity (lower seizure burden) is difficult to explain, but may suggest another action of astrocytic Ca²⁺ signals in the context of ictogenesis than promoting gliotransmitter release. If one considers SD as a potential mechanism for curbing seizure activity, and that this mechanism may partly explain the lower total amount of seizure activity in the *Itpr2*^{-/-} mouse model, impaired astrocytic K⁺ uptake in the knockout mice could be a mechanism linking the 2 observations. It has been shown that astrocytic Ca²⁺ signals may stimulate astrocytic Na⁺/K⁺ ATPase activity (Wang et al. 2012), effectively lowering extracellular K⁺ concentrations. Hence, the lack of astrocytic Ca²⁺ signals could in theory lead to higher extracellular K⁺ levels promoting seizure termination by SD. These hypotheses should be investigated in future studies.

Our findings are supported by results from Nedergaard and coworkers, who observed paroxysmal depolarization shifts in neurons as a result of astrocytic Ca²⁺ elevations, as well as stereotypical astrocytic Ca²⁺ signals during seizure activity (Tian et al. 2005). However, recently published data from an in vivo rat model for focal neocortical seizures (Baird-Daniel et al. 2017) conflict with our results. Baird-Daniel et al. reported that seizures were associated with a glial Ca²⁺ wave that was “markedly delayed after both neuronal and hemodynamic onset” and that this astrocytic Ca²⁺ elevation was of minor—if any—importance in ictogenesis. The discrepancies between their and our findings may rely on differences in experimental setups, including choice of species, chemoconvulsant and type

of Ca²⁺ indicator. Notably, Baird-Daniel et al. used less sensitive bulk-loaded synthetic Ca²⁺ dyes, as discussed below. Also, astrocyte heterogeneity and regional differences in network excitability may play a role. It is well established that hippocampal and cortical astrocytes differ in morphology and function, including neurotransmitter receptor expression and Ca²⁺ signaling (Oberheim et al. 2012). Distinct roles of hippocampal astrocytes, and particular properties in their Ca²⁺ mediated cell communication may explain why the hippocampus is especially seizure prone (Harris-White et al. 1998). Moreover, the study of Baird-Daniel et al. may be confounded by the use of anesthetics, as these markedly suppress astrocytic Ca²⁺ signaling (Thrane et al. 2012). Our in vivo experiments were conducted without the use of anesthesia.

While local hippocampal astrocytes were activated seconds before neurons during the first seizure, they were typically activated concomitantly or at varying time delays compared with local neurons in the following ictal episodes. Consequently, the tissue must have undergone pathophysiological and/or morphological changes as a direct result of the initial insult. A multitude of changes entailing time scales from milliseconds to minutes may occur upon the first ictal event that could perturb intrinsic interactions between astrocytes and neurons, and quickly increase network excitability (Henneberger 2017).

The first round of epileptiform activity was always terminated by a slowly propagating wave of high amplitude Ca²⁺ elevation in both neurons and astrocytes. Also, some subsequent bouts of epilepsy ended in a similar fashion. These waves matched the characteristics of SD waves as previously reported (Enger et al. 2015, 2017; Khoshkhoo et al. 2017), including SD

events in association with seizure activity observed in electrophysiological studies (Fabricius et al. 2008). Although the LFP measurement electrodes could not be placed directly in the field-of-view, characteristic DC-shifts were registered in association with such fluorescent waves. This observation is interesting not the least from a clinical point of view: the pathological phenomena of seizures and SD have been recognized to share essential pathophysiological features (Rogawski 2008; Dreier et al. 2012; Wei et al. 2014; Mantegazza and Cestè 2018). The hallmark of both migraine and epilepsy is a paroxysmal dysfunction of cellular/network excitability and, furthermore, both conditions are highly co-morbid and respond to antiepileptic drugs (Rogawski and Löscher 2004; Keezer et al. 2015).

Several mechanisms on different size scales are proposed to be involved in seizure termination, ranging from the single cell to local networks and brain-wide circuits (Lado and Moshé 2008; Kramer et al. 2012). Still, how seizures terminate remains one of the most important unanswered questions in epileptology (Lado and Moshé 2008). Our experiments provide the first in vivo visualization of concomitant occurrence of seizure activity and SD in the hippocampus, and perhaps more importantly, demonstrate that SD reliably terminates local neuronal activity. In SD models, it is well known that SD silences evoked synaptic activity for several minutes (for review: Lauritzen et al. 2011; Dreier et al. 2012)). Therefore, it is not surprising that SD also could depress epileptiform activity, and potentially contribute to seizure termination. Understanding the critical step towards the return to the interictal state could identify novel targets for therapeutic action. However, whether SD is an epiphenomenon of ictal activity or a compensatory mechanism to curb seizure activity remains to be determined.

Traditional bulk-loaded synthetic Ca²⁺ indicators only delineate the soma and largest processes of the astrocyte (Reeves et al. 2011; Leybaert and Sanderson 2012). However, astrocyte–neuron communication does not necessarily involve Ca²⁺ signals in the astrocytic soma, but may occur in processes and endfeet (Panatier et al. 2011; Szokol et al. 2015). Improved imaging techniques and the development of genetically encoded Ca²⁺ indicators now allow us to assess focal and small-scale Ca²⁺ transients in these subcellular compartments (Kanemaru et al. 2014; Srinivasan et al. 2015). In our study, we used the Ca²⁺ indicator GCaMP6f, which out-performs synthetic Ca²⁺ indicators both in terms of signal-to-noise ratio and to which degree they outline astrocytic territories (Srinivasan et al. 2015). Notably, we find higher rates of Ca²⁺ transients both during seizures and between bouts of seizures in astrocytic processes, highlighting a complexity of astrocytic Ca²⁺ signaling that would have been lost using bulk-loaded Ca²⁺ indicators.

Here, for the first time, we demonstrate an attenuated seizure burden in *Itp2*^{-/-} mice after exposure to kainate. The *Itp2*^{-/-} knockout mouse model has been used extensively to study the impact of astrocytic Ca²⁺ signals, but it is becoming more and more clear that these mice still exhibit astrocytic Ca²⁺ signals both in physiology (Srinivasan et al. 2015)—and to a larger extent—in pathophysiology (Enger et al. 2017). Notwithstanding, this mouse model lacks one of the main pathways that mediate intracellular Ca²⁺ elevations in astrocytes, and large synchronized Ca²⁺ elevations are absent during physiological stimuli in these mice. We found that the astrocytic preactivation observed in WT animals was abolished in the *Itp2*^{-/-} mice. We also showed that there was a strong reduction in astrocytic Ca²⁺ signaling in these mice, although prominent Ca²⁺ transients still were present. There was also a lower seizure burden when considering AUC of the neuronal Ca²⁺ signal. This tendency was

confirmed and underscored in a more sensitive essay comprising telemetric EEG monitoring, demonstrating a substantially lower seizure burden in the *Itp2*^{-/-} compared with WT.

IP₃ receptors are mediators of second messenger-induced intracellular Ca²⁺ release and 3 IP₃ receptor isoforms are known. IP3R2 is the predominant IP₃ receptor in glial cells, and is thought to be the key functional IP₃ receptor in astrocytes (Sharp et al. 1999; Foskett et al. 2007). Lack of IP3R2 has been shown to abolish both spontaneous and G_q-linked G-protein coupled receptor mediated increases in hippocampal astrocyte Ca²⁺ transients (Petraevicz et al. 2008). Regardless of the importance of IP₃ as second messenger for astrocytic Ca²⁺ dynamics, mice lacking IP3R2 are overtly normal (Petraevicz et al. 2008). Accordingly, several recent studies have questioned the physiological importance of astrocyte Ca²⁺ signaling, by for instance demonstrating normal synaptic transmission and plasticity in these mice (Aguilhon et al. 2010; Nizar et al. 2013; Petraevicz et al. 2014). Importantly, recent in vivo state-of-the art imaging techniques with new genetically encoded Ca²⁺ indicators (GCaMP6f, as used in this study) showed that Ca²⁺ fluctuations are not markedly altered in astrocyte processes of *Itp2*^{-/-} mice although Ca²⁺ signals in somata are strongly reduced (Srinivasan et al. 2015). Our data demonstrate a strong reduction of Ca²⁺ events also in astrocytic subcompartments, highlighting another difference between the seizing or interictal brain state compared with physiologic activation.

Interestingly, the reduction of AUC of the astrocytic Ca²⁺ signal in *Itp2*^{-/-} mice versus WT mice in endfeet failed to reach statistical significance ($P = 0.2$). In contrast, both duration and amplitude of these signals are significantly lower. The lack of effect of *Itp2*^{-/-} on the AUC in endfeet could imply that other mechanisms of Ca²⁺ increase than through IP₃-receptors play a relatively more important role in endfeet than in other astrocytic subcompartments. A likely explanation is that endfeet, due to their high expression of aquaporin-4 water channels (Nielsen et al. 1997), are more prone to glutamate- and potassium-induced swelling, and hence swelling-induced Ca²⁺ signals, than other astrocytic subcompartments. It is also possible that transient receptor potential cation channel subfamily V member 4 (TRPV4), a swelling-sensitive cation channel enriched in endfeet, mediates Ca²⁺ entry into endfeet during our experimental conditions (Jo et al. 2015; Toft-Bertelsen et al. 2018).

Although the downstream effects of astrocytic Ca²⁺ elevations remain unclear, it is worth noting that propagation speed of SD was markedly increased in *Itp2*^{-/-} mice. We have previously reported that SD waves triggered by elevated K⁺ also propagate faster in these knockouts than in WT mice (Enger et al. 2017). It is tempting to ascribe parts of the genotype differences in seizure activity to altered SD kinetics in the knockout mice.

Conclusion

We demonstrate that prominent astroglial Ca²⁺ activity precedes local neuronal activity during spread of kainate-induced seizures in the intact hippocampus of awake mice. This preactivation of glia is abolished in *Itp2*^{-/-} mice, which exhibit reduced epileptiform activity when compared with WT mice. In all, our data suggest a proconvulsive role of astrocytic Ca²⁺ elevations. The contribution of astrocytic Ca²⁺ signals are probably modulatory rather than an integral part of seizure propagation as *Itp2*^{-/-} mice with strongly attenuated Ca²⁺ signals in astrocytes still develop seizures. Nonetheless, this modulatory activity may leave astrocytic Ca²⁺ signaling a promising target for therapeutic intervention.

Supplementary Material

Supplementary material is available at *Cerebral Cortex* online.

Contributions

K.H. designed experiments, acquired and interpreted data, and wrote the article; C.G.N. designed experiments, acquired and analyzed data and edited the article. K.H.P. analyzed and interpreted data, and edited the article; V.J. designed experiments, acquired data, and edited the article; K.S.Á. made tools for data acquisition and analyses, and edited the article; W.T. designed and produced the fluorescent probes and contributed to study design and edited the article. R.S. designed the fluorescent probes, contributed to data interpretation, and edited the article; E.T. conceived the study, interpreted data, and edited the article; E.A.N. conceived the study, interpreted data, and edited the article. R.E. conceived the study, designed experiments, acquired, analyzed and interpreted data, and wrote the article.

Funding

The South-East Health Region of Norway (Grant #2013021 to E.A.N.), the Research Council of Norway (Grants 249988 and 240476 to E.A.N.), the Olav Thon Foundation (to E.A.N.), the Letten Foundation (to E.A.N.), the Max Planck Institute for Medical Research (to R.S.) and SFB 1134/B01 (to R.S.) and the European Commission, ERA-NET NEURON, Brain Inflammation, Glia and Epilepsy (to K.H.).

Notes

We thank Dr Øivind Skare for expert advice on the statistical analyses. We gratefully acknowledge the support by UNINETT Sigma2 AS, for making data storage available through NIRD, project NS9021K. *Conflicts of Interest:* The authors report no conflicts of interest.

References

- Agulhon C, Fiacco TA, McCarthy KD. 2010. Hippocampal short- and long-term plasticity are not modulated by astrocyte Ca^{2+} signaling. *Science*. 327:1250–1254.
- Agulhon C, Petracvic J, McMullen AB, Sweger EJ, Minton SK, Taves SR, Casper KB, Fiacco TA, McCarthy KD. 2008. What is the role of astrocyte calcium in neurophysiology? *Neuron*. 59:932–946.
- Aronica E, Ravizza T, Zurolo E, Vezzani A. 2012. Astrocyte immune responses in epilepsy. *Glia*. 60:1258–1268.
- Avoli M, de Curtis M. 2011. GABAergic synchronization in the limbic system and its role in the generation of epileptiform activity. *Prog Neurobiol*. 95:104–132.
- Azevedo FAC, Carvalho LRB, Grinberg LT, Farfel JM, Ferretti REL, Leite REP, Filho WJ, Lent R, Herculano-Houzel S. 2009. Equal numbers of neuronal and nonneuronal cells make the human brain an isometrically scaled-up primate brain. *J Comp Neurol*. 513:532–541.
- Baird-Daniel E, Daniel AGS, Wenzel M, Li D, Liou JY, Laffont P, Zhao M, Yuste R, Ma H, Schwartz TH. 2017. Glial calcium waves are triggered by seizure activity and not essential for initiating ictal onset or neurovascular coupling. *Cereb Cortex*. 27:3318–3330.
- Barrett MJP, Ferrari KD, Stobart JL, Holub M, Weber B. 2018. CHIPS: an extensible toolbox for cellular and hemodynamic two-photon image analysis. *Neuroinformatics*. 16:145–147.
- Bazargani N, Attwell D. 2016. Astrocyte calcium signaling: the third wave. *Nat Neurosci*. 19:182–189.
- Bedner P, Dupper A, Hüttmann K, Müller J, Herde MK, Dublin P, Deshpande T, Schramm J, Häussler U, Haas CA, et al. 2015. Astrocyte uncoupling as a cause of human temporal lobe epilepsy. *Brain*. 138:1208–1222.
- Bekar LK, He W, Nedergaard M. 2008. Locus coeruleus α -adren-ergic-mediated activation of cortical astrocytes in vivo. *Cereb Cortex*. 18:2789–2795.
- Ben-Ari Y, Cossart R. 2000. Kainate, a double agent that gener-ates seizures: two decades of progress. *Trends Neurosci*. 23: 580–587.
- Binder DK, Nagelhus EA, Ottersen OP. 2012. Aquaporin-4 and epilepsy. *Glia*. 60:1203–1214.
- Bushong EA, Martone ME, Jones YZ, Ellisman MH. 2002. Protoplasmic astrocytes in CA1 stratum radiatum occupy separate anatomical domains. *J Neurosci*. 22:183–192.
- Carmignoto G, Haydon PG. 2012. Astrocyte calcium signaling and epilepsy. *Glia*. 60:1227–1233.
- Carta M, Fièvre S, Gorlewicz A, Mulle C. 2014. Kainate receptors in the hippocampus. *Eur J Neurosci*. 39:1835–1844.
- Chen N, Sugihara H, Sharma J, Perea G, Petracvic J, Le C, Sur M. 2012. Nucleus basalis-enabled stimulus-specific plasticity in the visual cortex is mediated by astrocytes. *Proc Natl Acad Sci*. 109:E2832–E2841.
- Chen T-W, Wardill TJ, Sun Y, Pulver SR, Renninger SL, Baohan A, Schreiter ER, Kerr RA, Orger MB, Jayaraman V, et al. 2013. Ultrasensitive fluorescent proteins for imaging neuronal activity. *Nature*. 499:295–300.
- Coulter DA, Eid T. 2012. Astrocytic regulation of glutamate homeostasis in epilepsy. *Glia*. 60:1215–1226.
- Crunelli V, Carmignoto G. 2013. New vistas on astroglia in con-vulsive and non-convulsive epilepsy highlight novel astro-cyctic targets for treatment. *J Physiol*. 591:775–785.
- Dana H, Mohar B, Sun Y, Narayan S, Gordus A, Hasseman JP, Tsegaye G, Holt GT, Hu A, Walpita D, et al. 2016. Sensitive red protein calcium indicators for imaging neural activity. *Elife*. 5:e12727.
- Darstein M, Petralia RS, Swanson GT, Wenthold RJ, Heinemann SF. 2003. Distribution of kainate receptor subunits at hippo-campal mossy fiber synapses. *J Neurosci*. 23:8013–8019.
- Ding F, O'Donnell J, Thrane AS, Zeppenfeld D, Kang H, Xie L, Wang F, Nedergaard M. 2013. α 1-Adrenergic receptors medi-ate coordinated Ca^{2+} signaling of cortical astrocytes in awake, behaving mice. *Cell Calcium*. 54:387–394.
- Dombeck DA, Harvey CD, Tian L, Looger LL, Tank DW. 2010. Functional imaging of hippocampal place cells at cellular resolution during virtual navigation. *Nat Neurosci*. 13: 1433–1440.
- Dreier JP, Major S, Pannek HW, Woitzik J, Scheel M, Wiesenthal D, Martus P, Winkler MKL, Hartings JA, Fabricius M, et al. 2012. Spreading convulsions, spreading depolarization and epilepto-genesis in human cerebral cortex. *Brain*. 135:259–275.
- Eid T, Thomas MJ, Spencer DD, Rundén-Pran E, Lai JCK, Malthankar GV, Kim JH, Danbolt NC, Ottersen OP, De Lanerolle NC. 2004. Loss of glutamine synthetase in the human epileptogenic hippocampus: possible mechanism for raised extracellular glutamate in mesial temporal lobe epilepsy. *Lancet*. 363:28–37.
- Enger R, Dukefoss DB, Tang W, Pettersen KH, Bjørnstad DM, Helm PJ, Jensen V, Sprengel R, Vervaeke K, Ottersen OP, et al. 2017. Deletion of aquaporin-4 curtails extracellular glu-tamate elevation in cortical spreading depression in awake mice. *Cereb Cortex*. 27:24–33.

- Enger R, Tang W, Vindedal GF, Jensen V, Helm PJ, Sprengel R, Looger LL, Nagelhus EA. 2015. Dynamics of ionic shifts in cortical spreading depression. *Cereb Cortex*. 25:4469–4476.
- Fabricius M, Fuhr S, Willumsen L, Dreier JP, Bhatia R, Boutelle MG, Hartings JA, Bullock R, Strong AJ, Lauritzen M. 2008. Association of seizures with cortical spreading depression and peri-infarct depolarisations in the acutely injured human brain. *Clin Neurophysiol*. 119:1973–1984.
- Fellin T, Gomez-Gonzalo M, Gobbo S, Carmignoto G, Haydon PG. 2006. Astrocytic glutamate is not necessary for the generation of epileptiform neuronal activity in hippocampal slices. *J Neurosci*. 26:9312–9322.
- Fellin T, Haydon PG. 2005. Do astrocytes contribute to excitation underlying seizures? *Trends Mol Med*. 11:530–533.
- Foskett JK, White C, Cheung K-H, Mak D-OD. 2007. Inositol triphosphate receptor Ca²⁺ release channels. *Physiol Rev*. 87:593–658.
- Grasse DW, Karunakaran S, Moxon KA. 2013. Neuronal synchrony and the transition to spontaneous seizures. *Exp Neurol*. 248:72–84.
- Gynther M, Petsalo A, Hansen SH, Bunch L, Pickering DS. 2015. Blood–brain barrier permeability and brain uptake mechanism of kainic acid and dihydrokainic acid. *Neurochem Res*. 40:542–549.
- Gómez-Gonzalo M, Losi G, Chiavogato A, Zonta M, Cammarota M, Brondi M, Vetri F, Uva L, Pozzan T, de Curtis M, et al. 2010. An excitatory loop with astrocytes contributes to drive neurons to seizure threshold. *PLoS Biol*. 8:e1000352.
- Halassa MM, Haydon PG. 2010. Integrated brain circuits: astrocytic networks modulate neuronal activity and behavior. *Annu Rev Physiol*. 72:335–355.
- Harris-White ME, Zanotti SA, Frautschy SA, Charles AC. 1998. Spiral intercellular calcium waves in hippocampal slice cultures. *J Neurophysiol*. 79:1045–1052.
- Henneberger C. 2017. Does rapid and physiological astrocyte–neuron signalling amplify epileptic activity? *J Physiol*. 595:1917–1927.
- Jabs R, Kirchhoff F, Kettenmann H, Steinhäuser C. 1994. Kainate activates Ca²⁺-permeable glutamate receptors and blocks voltage-gated K⁺ currents in glial cells of mouse hippocampal slices. *Pflüg Arch Eur J Physiol*. 426:310–319.
- Jo AO, Ryskamp DA, Phuong TTT, Verkman AS, Yarishkin O, MacAulay N, Križaj D. 2015. TRPV4 and AQP4 channels synergistically regulate cell volume and calcium homeostasis in retinal muller glia. *J Neurosci*. 35:13525–13537.
- Kaifosh P, Lovett-Barron M, Turi GF, Reardon TR, Losonczy A. 2013. Septo-hippocampal GABAergic signaling across multiple modalities in awake mice. *Nat Neurosci*. 16:1182–1184.
- Kanemaru K, Sekiya H, Xu M, Satoh K, Kitajima N, Yoshida K, Okubo Y, Sasaki T, Moritoh S, Hasuwa H, et al. 2014. *In vivo* visualization of subtle, transient, and local activity of astrocytes using an ultrasensitive Ca²⁺ indicator. *Cell Rep*. 8:311–318.
- Keezer MR, Bauer PR, Ferrari MD, Sander JW. 2015. The comorbid relationship between migraine and epilepsy: a systematic review and meta-analysis. *Eur J Neurol*. 22:1038–1047.
- Khoshkhoo S, Vogt D, Sohal VS. 2017. Dynamic, cell-type-specific roles for GABAergic interneurons in a mouse model of optogenetically inducible seizures. *Neuron*. 93:291–298.
- Klein P, Dingledine R, Aronica E, Bernard C, Blümcke I, Boison D, Brodie MJ, Brooks-Kayal AR, Engel J, Forcelli PA, et al. 2018. Commonalities in epileptogenic processes from different acute brain insults: do they translate? *Epilepsia*. 59:37–66.
- Kramer MA, Truccolo W, Eden UT, Lepage KQ, Hochberg LR, Eskandar EN, Madsen JR, Lee JW, Maheshwari A, Halgren E, et al. 2012. Human seizures self-terminate across spatial scales via a critical transition. *Proc Natl Acad Sci*. 109:21116–21121.
- Lado FA, Moshé SL. 2008. How do seizures stop? *Epilepsia*. 49:1651–1664.
- Lauritzen M, Dreier JP, Fabricius M, Hartings JA, Graf R, Strong AJ. 2011. Clinical relevance of cortical spreading depression in neurological disorders: migraine, malignant stroke, subarachnoid and intracranial hemorrhage, and traumatic brain injury. *J Cereb Blood Flow Metab*. 31:17–35.
- Leybaert L, Sanderson MJ. 2012. Intercellular Ca²⁺ waves: mechanisms and function. *Physiol Rev*. 92:1359–1392.
- Li X, Zima AV, Sheikh F, Blatter LA, Chen J. 2005. Endothelin-1-induced arrhythmogenic Ca²⁺ signaling is abolished in atrial myocytes of inositol-1,4,5-trisphosphate(IP₃)-receptor type 2-deficient mice. *Circ Res*. 96:1274–1281.
- Librizzi L, Losi G, Marcon I, Sessolo M, Scalmani P, Carmignoto G, de Curtis M. 2017. Interneuron network activity at the onset of seizure-like events in entorhinal cortex slices. *J Neurosci*. 37:10398–10407.
- Lindén H, Tetzlaff T, Potjans TC, Pettersen KH, Grün S, Diesmann M, Einevoll GT. 2011. Modeling the spatial reach of the LFP. *Neuron*. 72:859–872.
- Lovett-Barron M, Kaifosh P, Kheirbek MA, Danielson N, Zaremba JD, Reardon TR, Turi GF, Hen R, Zemelman BV, Losonczy A. 2014. Dendritic inhibition in the hippocampus supports fear learning. *Science*. 343:857–863.
- Mantegazza M, Cestè S. 2018. Pathophysiological mechanisms of migraine and epilepsy: similarities and differences. *Neurosci Lett*. 667:92–102.
- Melyan Z, Wheal HV, Lancaster B. 2002. Metabotropic-mediated kainate receptor regulation of IsAHP and excitability in pyramidal cells. *Neuron*. 34:107–114.
- Monaghan DT, Cotman CW. 1982. The distribution of [3H]kainic acid binding sites in rat CNS as determined by autoradiography. *Brain Res*. 252:91–100.
- Nathanson JL, Yanagawa Y, Obata K, Callaway EM. 2009. Preferential labeling of inhibitory and excitatory cortical neurons by endogenous tropism of adeno-associated virus and lentivirus vectors. *Neuroscience*. 161:441–450.
- Nedergaard M, Verkhratsky A. 2012. Artifact versus reality—how astrocytes contribute to synaptic events. *Glia*. 60:1013–1023.
- Nielsen S, Nagelhus EA, Amiry-Moghaddam M, Bourque C, Agre P, Ottersen OP. 1997. Specialized membrane domains for water transport in glial cells: high-resolution immunogold cytochemistry of aquaporin-4 in rat brain. *J Neurosci*. 17:171–180.
- Nimmerjahn A, Mukamel EA, Schnitzer MJ. 2009. Motor behavior activates Bergmann glial networks. *Neuron*. 62:400–412.
- Nizar K, Uhlirva H, Tian P, Saisan PA, Cheng Q, Reznichenko L, Weldy KL, Steed TC, Sridhar VB, MacDonald CL, et al. 2013. *In vivo* stimulus-induced vasodilation occurs without IP₃ receptor activation and may precede astrocytic calcium increase. *J Neurosci*. 33:8411–8422.
- Oberheim NA, Goldman SA, Nedergaard M. 2012. Heterogeneity of astrocytic form and function. *Methods Mol Biol*. 814:23–45.
- Panatier A, Vallée J, Haber M, Murai KK, Lacaille J-C, Robitaille R. 2011. Astrocytes are endogenous regulators of basal transmission at central synapses. *Cell*. 146:785–798.

- Parpura V, Basarsky TA, Liu F, Jęftinija K, Jęftinija S, Haydon PG. 1994. Glutamate-mediated astrocyte–neuron signalling. *Nature*. 369:744–747.
- Parpura V, Verkhratsky A. 2013. Astroglial amino acid-based transmitter receptors. *Amino Acids*. 44:1151–1158.
- Paukert M, Agarwal A, Cha J, Doze VA, Kang JU, Bergles DE. 2014. Norepinephrine controls astroglial responsiveness to local circuit activity. *Neuron*. 82:1263–1270.
- Perea G, Araque A. 2005. Properties of synaptically evoked astrocyte calcium signal reveal synaptic information processing by astrocytes. *J Neurosci*. 25:2192–2203.
- Perea G, Navarrete M, Araque A. 2009. Tripartite synapses: astrocytes process and control synaptic information. *Trends Neurosci*. 32:421–431.
- Perea G, Sur M, Araque A. 2014. Neuron–glia networks: integral gear of brain function. *Front Cell Neurosci*. 8:378.
- Petravic J, Boyt KM, McCarthy KD. 2014. Astrocyte IP₃R2-dependent Ca²⁺ signaling is not a major modulator of neuronal pathways governing behavior. *Front Behav Neurosci*. 8:384.
- Petravic J, Fiacco TA, McCarthy KD. 2008. Loss of IP₃ receptor-dependent Ca²⁺ increases in hippocampal astrocytes does not affect baseline CA1 pyramidal neuron synaptic activity. *J Neurosci*. 28:4967–4973.
- Pnevmatikakis EA, Giovannucci A. 2017. NoRMCorre: an online algorithm for piecewise rigid motion correction of calcium imaging data. *J Neurosci Methods*. 291:83–94.
- Porter JT, McCarthy KD. 1996. Hippocampal astrocytes in situ respond to glutamate released from synaptic terminals. *J Neurosci*. 16:5073–5081.
- Reeves AMB, Shigetomi E, Khakh BS. 2011. Bulk loading of calcium indicator dyes to study astrocyte physiology: key limitations and improvements using morphological maps. *J Neurosci*. 31:9353–9358.
- Rogawski MA. 2008. Common pathophysiologic mechanisms in migraine and epilepsy. *Arch Neurol*. 65:709–714.
- Rogawski MA, Löscher W. 2004. The neurobiology of antiepileptic drugs for the treatment of nonepileptic conditions. *Nat Med*. 10:685–692.
- Ruiz A. 2005. Distinct subunits in heteromeric kainate receptors mediate ionotropic and metabotropic function at hippocampal mossy fiber synapses. *J Neurosci*. 25:11710–11718.
- Schummers J, Yu H, Sur M. 2008. Tuned responses of astrocytes and their influence on hemodynamic signals in the visual cortex. *Science*. 320:1638–1643.
- Sharp AH, Nucifora FC, Blondel O, Sheppard CA, Zhang C, Snyder SH, Russell JT, Ryugo DK, Ross CA. 1999. Differential cellular expression of isoforms of inositol 1,4,5-triphosphate receptors in neurons and glia in brain. *J Comp Neurol*. 406:207–220.
- Sherwood CC, Stimpson CD, Raghanti MA, Wildman DE, Uddin M, Grossman LI, Goodman M, Redmond JC, Bonar CJ, Erwin JM, et al. 2006. Evolution of increased glia–neuron ratios in the human frontal cortex. *Proc Natl Acad Sci*. 103:13606–13611.
- Smith RH, Levy JR, Kotin RM. 2009. A simplified baculovirus–AAV expression vector system coupled with one-step affinity purification yields high-titer rAAV stocks from insect cells. *Mol Ther*. 17:1888–1896.
- Srinivasan R, Huang BS, Venugopal S, Johnston AD, Chai H, Zeng H, Golshani P, Khakh BS. 2015. Ca²⁺ signaling in astrocytes from *Ip3r2*^{-/-} mice in brain slices and during startle responses in vivo. *Nat Neurosci*. 18:708–717.
- Steinhäuser C, Grunnet M, Carmignoto G. 2016. Crucial role of astrocytes in temporal lobe epilepsy. *Neuroscience*. 323:157–169.
- Steinhäuser C, Seifert G, Bedner P. 2012. Astrocyte dysfunction in temporal lobe epilepsy: K⁺ channels and gap junction coupling. *Glia*. 60:1192–1202.
- Szokol K, Heuser K, Tang W, Jensen V, Enger R, Bedner P, Steinhäuser C, Taubä, ll E, Ottersen OP, Nagelhus EA. 2015. Augmentation of Ca²⁺ signaling in astrocytic endfeet in the latent phase of temporal lobe epilepsy. *Front Cell Neurosci*. 9:49.
- Takata N, Mishima T, Hisatsune C, Nagai T, Ebisui E, Mikoshiba K, Hirase H. 2011. Astrocyte calcium signaling transforms cholinergic modulation to cortical plasticity in vivo. *J Neurosci*. 31:18155–18165.
- Tang W, Ehrlich I, Wolff SBE, Michalski A-M, Wolff S, Hasan MT, Luthi A, Sprengel R. 2009. Faithful expression of multiple proteins via 2A-peptide self-processing: a versatile and reliable method for manipulating brain circuits. *J Neurosci*. 29:8621–8629.
- Thrane AS, Rangroo Thrane V, Zeppenfeld D, Lou N, Xu Q, Nagelhus EA, Nedergaard M. 2012. General anesthesia selectively disrupts astrocyte calcium signaling in the awake mouse cortex. *Proc Natl Acad Sci*. 109:18974–18979.
- Tian GF, Azmi H, Takano T, Xu Q, Peng W, Lin J, Oberheim NA, Lou N, Wang X, Zielke HR, et al. 2005. An astrocytic basis of epilepsy. *Nat Med*. 11:973–981.
- Toft-Bertelsen TL, Larsen BR, MacAulay N. 2018. Sensing and regulation of cell volume—we know so much and yet understand so little: TRPV4 as a sensor of volume changes but possibly without a volume-regulatory role? *Channels*. 12:100–108.
- Toyoda I, Fujita S, Thamattoor AK, Buckmaster PS. 2015. Unit activity of hippocampal interneurons before spontaneous seizures in an animal model of temporal lobe epilepsy. *J Neurosci*. 35:6600–6618.
- Truccolo W, Donoghue JA, Hochberg LR, Eskandar EN, Madsen JR, Anderson WS, Brown EN, Halgren E, Cash SS. 2011. Single-neuron dynamics in human focal epilepsy. *Nat Neurosci*. 14:635–643.
- Vargas JR, Takahashi DK, Thomson KE, Wilcox KS. 2013. The expression of kainate receptor subunits in hippocampal astrocytes after experimentally induced status epilepticus. *J Neuropathol Exp Neurol*. 72:919–932.
- Wang F, Smith NA, Xu Q, Fujita T, Baba A, Matsuda T, Takano T, Bekar L, Nedergaard M. 2012. Astrocytes modulate neural network activity by Ca²⁺-dependent uptake of extracellular K⁺. *Sci Signal*. 5:ra26.
- Wei Y, Ullah G, Schiff SJ. 2014. Unification of neuronal spikes, seizures, and spreading depression. *J Neurosci*. 34:11733–11743.
- Zaremba JD, Diamantopoulou A, Danielson NB, Grosmark AD, Kaifosh PW, Bowler JC, Liao Z, Sparks FT, Gogos JA, Losonczy A. 2017. Impaired hippocampal place cell dynamics in a mouse model of the 22q11.2 deletion. *Nat Neurosci*. 20:1612–1623.
- Zhang M, Ladas TP, Qiu C, Shivacharan RS, Gonzalez-Reyes LE, Durand DM. 2014. Propagation of epileptiform activity can be independent of synaptic transmission, gap junctions, or diffusion and is consistent with electrical field transmission. *J Neurosci*. 34:1409–1419.